Energy 313 (2024) 134005

Contents lists available at ScienceDirect

Energy

journal homepage: www.elsevier.com/locate/energy

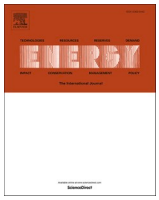

Cost-optimal design of reverse electrodialysis process for salinity gradient-based electricity generation in desalination plants

C. Tristán [a,*], M. Fallanza [a], I. Ortiz [a], R. Ibáñez [a], I.E. Grossmann [b]

[a] Department of Chemical and Biomolecular Engineering, University of Cantabria, Av. Los Castros 46, 39005, Santander, Spain
[b] Department of Chemical Engineering. Carnegie Mellon University, Pittsburgh, PA, 15213, USA

ARTICLE INFO

Handling editor: Henrik Lund

Keywords:
Renewable energy
Generalized disjunctive programming
Reverse osmosis
Wastewater treatment
Water-energy nexus

ABSTRACT

Salinity gradient-based technologies offer a solution for desalination plants seeking clean, uninterrupted electricity to support their decarbonization and circularity. This work provides cost-optimal designs of a large-scale reverse electrodialysis (RED) system deployed in a desalination plant using mathematical programming. The optimization model determines the hydraulic topology and RED units' working conditions that maximize the net present value (NPV) of the RED process recovering salinity gradient energy between brine and treated wastewater effluents. We examine how electricity, carbon and membranes prices, desalination plant capacity, and membrane resistance may affect the NPV-optimal design's competitiveness and performance. We also compare the conventional series-parallel configuration and the NPV-optimal solution with recycling and added reuse alternatives. In the context of soaring electricity prices and strong green financing support, with the use of high-performing, affordable membranes (~10 €/m^2), RED could save 8 % of desalination plant energy demand from the grid, earning 5 M€ profits and LCOE of 66–126 €/MWh, comparable to other renewable and conventional power technologies. The optimization model finds profitable designs for the entire range of medium-capacity desalination plants. The findings underscore the optimization model effectiveness in streamlining decision-making and exploiting the synergies of full-scale, RED-based electricity in the energy-intensive water sector.

1. Introduction

The energy released by mixing two water streams of different salinities, so-called salinity gradient energy (SGE), is a vast yet largely untapped renewable power source [1,2] to complement and diversify the current carbon and water-intensive energy mix [3,4], and sustain the energy-intensive water sector [5]. SGE technologies offer an integrated approach to the United Nations' Sustainable Development Goal (SDG) 7 on affordable, reliable, sustainable energy access, and SDG 6 on clean water and sanitation.

Desalination and wastewater reuse are projected to increase in the coming decades [6,7] to reduce withdrawals from conventional surface and groundwater resources, while meeting stringent water quality standards. However, as large energy users of conventional power sources [8], they are also large greenhouse gas (GHG) emitters that question their sustainability [9]. Seawater reverse osmosis (SWRO), the technology of choice in the global desalination market [10], is getting closer to the practical minimum energy to desalinate seawater hitting a record, low specific energy consumption (SEC) of ~2 kWh/m^3 of desalted water [11]. Despite the marked decline in SEC, the carbon footprint of large-scale desalination plants remains an issue [12,13]. Hence, coupling desalination with renewable energy sources will be vital for the sustainable production of desalinated water [14]. SGE technologies can provide clean, base-load electricity to desalination and wastewater treatment plants, supporting their decarbonization and circularity [5].

Within the SGE technologies, reverse electrodialysis (RED) has made great progress in the past two decades, and is now closer to commercialization with some pilot trials [15–17] and field demonstrations [18–20]. In principle, a RED system takes in low- and high-salinity waters (LC and HC) on either side of alternate pairs of cation-exchange (CEM) and anion-exchange (AEM) membranes that let through counter-ions, but not co-ions and water [21]. The salinity difference over each ion-exchange membrane (IEM) creates an electrochemical potential that drives the diffusion of cations through CEMs towards the cathode, and anions through AEMs towards the anode from the saltier stream to the less-salty side; redox reactions at the outer electrodes convert this ionic flow into an electron flux. The electric potential of the membrane pile and the resulting electric current can

* Corresponding author.
E-mail address: tristanc@unican.es (C. Tristán).

https://doi.org/10.1016/j.energy.2024.134005
Received 17 June 2023; Received in revised form 4 September 2024; Accepted 25 November 2024
Available online 28 November 2024

then be used to power the external load.

Using natural underground seawater and treated municipal wastewater from a local treatment plant in Jeju (South Korea), Nam et al. [15] tested a pilot-scale RED stack with 1000 cell pairs of IEMs. The stack had a total membrane area of 250 m^2 and generated a gross power of 95.8 W. The presence of multivalent ions and natural organic matter result in a low power density (0.38 W/m^2 total membrane) and energy conversion efficiency of 11.4 %–13.3 % [15]. Yasukawa et al. [16] assessed a small-scale RED system with 200 cells and 40 m^2 of membrane surface area, using real brine from the Mamizu Pia SWRO desalination plant and effluent from the Wagiro sewage treatment plant in Fukuoka, Japan. They found a net power output of 18.2 W (net power density of 0.46 W/m^2) and an energy conversion efficiency of 17–26 %. Later on, Mehdizadeh and colleagues [17] assessed the performance of a RED stack consisting of 299 cell pairs and a membrane effective area of 179.4 m^2. The stack was run using brine from the Okinawa SWRO desalination plant and surface water, resulting in a net power output of 143.6 W (0.80 W/m^2). The authors suggest that if the Okinawa desalination plant releases 60,000 m3 of brine daily, it could produce a net power of 437 kW per day. The Afsluitdijk in the Netherlands became home to the REDstack BV demonstration plant at Technology Readiness Level (TRL) 7 in 2014, marking a major milestone. Using a mixture of salt water (28 g/L) from the Wadden Sea and freshwater (0.2–0.5 g/L) from Lake IJssel, this plant operates stacks with a total membrane area of 250 m^2 and is currently producing 50 kW [19,20]. In Trapani, Italy, the REAPower pilot plant is another demonstration project currently non-operational. It harnessed the power of natural saturated brine (5 M) from the nearby saltworks and brackish water (30 mM) from a shoreline well, producing a total of 330 W (total net power density of 0.75 W/m^2) from three RED stacks with a combined membrane area exceeding 400 m^2 [22].

The low power density of large-scale RED (0.38–2.7 W/m^2 total membrane area), fouling, and high cost of commercial membranes are the main limitations for RED technological readiness [1,23]. The benchmark for RED to be on par with other renewable energy sources is a sustained net power density of 2 W/m^2 at 40 % energy efficiency [19]. Niche markets beyond utility-scale electricity open new avenues to prove and advance RED market readiness [24]. For instance, seawater desalination brine and wastewater are discarded streams that can be exploited to produce and save energy while minimizing the environmental impact of brine disposal [25]. Besides, desalination's seawater influent is already pre-treated to remove foulants [26], so the rejected brine would likely be less prone to cause fouling than raw seawater, which would require further energy-intensive purification.

Several simulation and optimization studies have investigated designs and operating conditions that maximize the net power density [27–29], along with energy efficiency [30] of a single RED stack or several RED units in series [31–33] or simple layouts [34–36]. Few have considered more complex topologies and cost metrics (*e.g.*, net present value, levelized cost of electricity), which are key drivers for widespread RED adoption [23]. Designing for the RED process involves multiple variables and constraints, making it more difficult to find the most cost-efficient solutions using heuristics. An alternative to making decisions about RED process design is to use optimization-based methods that rigorously search for the optimal configuration in a given design space [37,38]. Notably, Generalized Disjunctive Programming (GDP) is a higher-level modeling framework that makes the formulation process more intuitive and systematic, while preserving the underlying logic structure of the problem in the model [39]. Tristán et al. [40] developed a GDP optimization model that incorporates a detailed model of the RED stack [41,42] to define the hydraulic topology and the working conditions of a set of RED units that maximize the net present value (NPV) of the RED process. Our work illustrates the functionality and benefits of mathematical programming and GDP modeling on the conceptual design and optimization of small-scale RED process over conventional heuristics.

Niche market for testing and promoting RED on a large scale is electricity generation from brines. Yet, the intricate design and operation space of the growing number of RED units requires optimization-based methods to effectively handle the challenge. In this follow-up study, we apply our GDP optimization model [40] to define the cost-optimal design of a large-scale RED system in a SWRO desalination plant. In addition, we explore how electricity and emissions allowances prices over time, membranes price, SWRO desalination plant capacity, and membranes resistance, may affect the cost-optimal design, economic feasibility, and competitiveness of the RED process using advanced mathematical programming tools, which is barely addressed in the open literature. To evaluate the benefits of the GDP model over heuristics, we also compare the conventional series-parallel configuration with the optimal solution to the GDP problem, which includes recycling and reuse alternatives of the RED units' exhausted streams. This case study serves to gauge the emissions and energy savings from the water- and carbon-intensive grid mix the RED system can offer to desalination in the most cost-conscious way, the way forward to make RED-based electricity a full-scale reality.

2. Methods

Optimization-based strategies involve three major steps: (i) postulating a superstructure that embeds the relevant flowsheet alternatives from which the optimum solution is selected, (ii) its formulation as a tractable mathematical programming model; and (iii) solving the model with an optimization algorithm to determine the optimal configuration [37,43]. Since the GDP model for the optimal design of the RED process is thoroughly described in Ref. [40], we will brief the reader on the main equations and assumptions.

2.1. Problem statement and superstructure definition

The problem addressed is to determine the hydraulic topology, that is, the number and hydraulic arrangement of the RED units and their working conditions (*e.g.*, electric current, inlet flow velocities, and molar concentrations) that yield the cost-optimal flowsheet design of the RED process for a given concentration, volume, and temperature of the high-salinity and low-salinity feed streams, and a fixed design of the RED stacks.

The superstructure in Fig. 1 displays the feasible design alternatives for the stated problem, *i.e.*, RED-based electricity production from the embedded energy of the HC and LC feed waste streams, with a given number of conditional RED units, $N_r = 2$. The representation of alternatives consists of: (i) sets of units $u \in \{FSU, RSU, RU, RMU, DMU\}$; (ii) sets of inlet and outlet ports or mixers and splitters, $p \in P = P_{out} \cup P_{in}$, where flows of material may take place; and (iii) sets of streams or feasible connections between outlet and inlet ports, $s \in S \subseteq P_{out} \times P_{in}$.

In Fig. 1, the HC and LC feed units, $fs \in FSU$, supply the high- and low-concentration feedwaters, $sol \in SOL = \{HC, LC\}$, to the RED Process Unit (RPU). The source units $rm \in RMU$ in the RPU parent block transfer HC and LC feedstreams from the feed units, *FSU*, to one or more of the candidate RED units, $r \in RU = \{r1, \ldots, rN_r\}$. After the active RED units have retrieved SGE from the inlet streams, the diluted HC and concentrated LC spent effluents can either be recycled back into other active RED units, reused, or directed to the sink units, $rm \in RMU$, where the RPU's exhausted HC and LC effluents are disposed of in the corresponding overall discharge units, $dm \in DMU$. Rather than passing through the RPU, the leftover feeds from *FSU* are directed straight to *DMU* for disposal, meaning feedstreams from *RMU* must go through the active RED units to recover SGE before reaching *RSU*. The transfer of ions from high-salinity to low-salinity compartments across membranes during SGE conversion is the only way for HC and LC waters to mix within the candidate RED units.

The reader is referred to Ref. [40] and Supplementary data for details on the superstructure definition and notation.

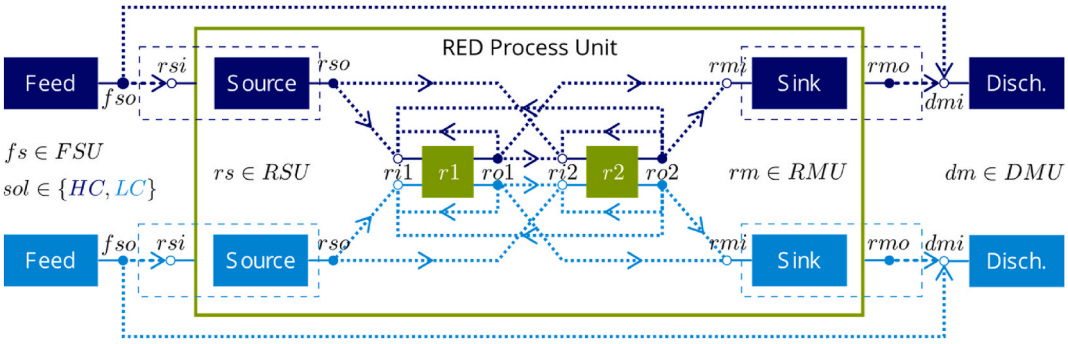

Fig. 1. Superstructure for the RED process with two candidate RED units. High (HC) and low-salinity (LC) feed ($fs \in FSU$) and discharge ($dm \in DMU$) units. The set of source ($rs \in RSU$) and sink ($rm \in RMU$) units and the set of candidate RED units ($r \in RU$) are children of the parent RED Process unit (RPU).

2.2. Optimization model

The set of equations (1) describes the Generalized Disjunctive Programming (GDP) optimization model for the superstructure in Fig. 1. GDP models involve continuous and Boolean variables with constraints in the form of algebraic expressions, conditional constraints within disjunctions, and logical propositions. The N_r two-term disjunctions represent the discrete activation and deactivation of the N_r candidate RED units. In problem (1), the objective is to maximize the Net Present Value (NPV) of the RED process subject to inequality constraints from process specifications and equality constraints from material, energy balances, and thermodynamic relationships. The continuous variables x are the molar concentrations and volumetric flows of the streams, and the internal variables of the active RED units. Decisions are made on the electric current and the concentration and flowrate of the RED stack's inlet streams.

$$\begin{aligned} \max_{x,Y_r} NPV = \quad & f(x) \\ s.t. \quad & g(x) \le 0 \\ & \begin{bmatrix} Y_r \\ h_r(x) \le 0 \end{bmatrix} \veebar \begin{bmatrix} \neg Y_r \\ B^r x = 0 \end{bmatrix} \quad \forall r \in RU \\ & \Omega(Y_r) = True \\ & x \in X \subseteq R^n \\ & Y_r = \{True, False\}^p \end{aligned} \tag{1}$$

The global constraints outside the disjunctions, $g(x) \le 0$ equation (S1) in Supplementary data, are equalities and inequalities describing specifications and physical relationships that apply for all feasible configurations in the superstructure, *e.g.*, mass balances of the feed, source, sink, and discharge units, and the upper and lower bounds on concentration and flowrate. In each term of the disjunctions, the Boolean variables Y_r define the existence or absence of the RED unit; if a unit exists or is selected ($Y_r = True$), the associated active constraints $h_r(x) \le 0$ in (S2) impose the relevant mass and energy balances or other physicochemical phenomena that apply in the RED unit ($r_r(x) \le 0$), add the incurred capital and operating cost to the objective function, and set lower and upper bounds on its internal variables and the concentration and flowrate of its inlet and outlet streams; otherwise, the negation ($\neg Y_r$) ignores the RED unit equations in the inactive disjunctive term, and $B^r x = 0$ constraints in (S3) set to zero a subset of the continuous variables and cost terms in the objective function. Other types of logical relationships for selecting the candidate RED units ($\Omega(Y_r) = True$) are specified using logic propositions.

To formulate the GDP problem, we assume.

(a) The feed streams are pure sodium chloride (NaCl) solutions, thus neglecting the non-idealities of aqueous solution (*i.e.*, unity activity coefficients) and the existence of other species that would undermine the RED performance.
(b) The internal losses depend only on the ionic resistance of solutions and membranes.
(c) Constant membranes permselectivity and ionic resistance apply, regardless of the solutions concentration and temperature.
(d) There is no water transport across the membranes against the concentration gradient due to osmosis, which implies a constant streamwise volumetric flowrate in RED's channel.
(e) Salt diffusivities in the membrane phase are independent of solutions concentration and temperature.
(f) No fluid leakage or ionic shortcut currents in the RED stack's manifolds.
(g) Co-current flow of the high- and low-concentration streams.
(h) The RED system operates under isothermal and isobaric conditions.

The solution to the GDP model maximizes the NPV of the RED process (2), which considers operating (OPEX in €/year), and capital costs (CAPEX in €) annualized over the expected lifetime of the plant LT in years, using the capital recovery factor, CRF, given in (4) with a discount rate DR. The OPEX and annualized CAPEX define the total annual cost (3), TAC, of the RED system. The NPV accounts for electricity sales and carbon pricing revenues. The RED plant electricity is sold to the grid at Spanish average price of electricity for non-house consumers, ep [44], and the abated GHG emissions from the grid mix (Spanish emission factor, ef [45]) are subsidized at the average price, cp, in the European Union Emission Trading System (EU ETS) [46].

We use a semi-rigorous version of Tristán et al. [40,41] RED stack model, to balance model fidelity and tractability. When the RED unit is active ($Y_r = True$), the discretized model $r_r(x) \le 0$ in (S2) predicts the net power output, NP_r, that is added to the net power capacity of the RED system, *i.e.*, total net power, TNP in kW (5). When the RED unit is absent ($\neg Y_r$) the net power output is set to zero.

We consider plant downtime due to membrane cleaning and system maintenance by applying a load factor, LF, to the annual energy yield (kWh/year) of the RED plant working at full capacity.

$$NPV = \frac{(ep + cp{\cdot}ef)\ TNP\ 8760\ LF - TAC}{CRF} \tag{2}$$

$$TAC = CRF{\cdot}CAPEX + OPEX \tag{3}$$

$$CRF = \frac{DR}{1 - (1 + DR)^{-LT}} \tag{4}$$

$$TNP = \sum_{r \in RU} NP_r \tag{5}$$

To estimate the capital investment in (6), we determine the cost of RED stacks, $\sum_{r \in RU} CC_{stack,r}$, pumps, CC_{pump}, and civil and electrical

infrastructure costs, CC_{civil}.

$$CAPEX = \sum_{r\in RU} CC_{stack,r} + CC_{pump} + CC_{civil} \tag{6}$$

The annual operating cost (7) comprises the electricity cost from pumps, $\sum_{r\in RU} OC_{pump,r}$, the replacement cost of membranes, $\sum_{r\in RU} OC_{IEMsrep,r}$, and maintenance and labor costs (as 2 % of CAPEX [47]).

$$OPEX = \sum_{r\in RU} OC_{pump,r} + \sum_{r\in RU} OC_{IEMsrep,r} + 0.02\ CAPEX \tag{7}$$

When the RED unit is active, $CC_{stack,r}$ in (S2) is added to CAPEX, and $OC_{pump,r}$ and $OC_{IEMsrep}$ in (S2) to OPEX; otherwise, these terms take zero values.

The objective function in (2) is maximized subject to constraints in the GDP that are detailed in Tristán et al. [40] and Supplementary data. The remainder financial parameters are those reported in Table 1.

2.3. Solution strategy

We code the GDP model using the Python-based, algebraic modeling language Pyomo [49] and Pyomo.GDP, a Pyomo library extension for logic-based modeling and optimization [50]. To solve the GDP problem, we apply the Global Logic-based Outer Approximation (GLOA) algorithm [51,52] implemented in the logic-based solver GDPopt version 20.2.28 built on Pyomo.GDP. The GLOA algorithm decomposes the solution to the GDP into a sequence of mixed-integer linear programming (MILP) master problems and reduced nonlinear programming (NLP) subproblems.

We solve the MILP master problems with CPLEX and the NLP subproblems with the multistart heuristic algorithm MSNLP using IPOPTH as a local NLP solver on a machine running Windows 10 (x64) with 6 cores processor (Intel® Core™ i7-8700 CPU @3.2 GHz) and 16 GB of RAM. We access the MINLP and NLP solvers from GAMS 34.1.0 through the Pyomo-GAMS interface. The stopping criteria depend upon the specified MSNLP solver's maximum number of iterations to guarantee a near-optimal solution.

2.4. Techno-economic performance metrics

To assess the technical performance of the optimal RED process designs, we determine its net power density, *i.e.*, the net power produced per membrane area, and its net energy efficiency, or the fraction of exergy or theoretical maximum energy attainable in form of SG, converted to useful work. We consider the Levelized Cost of Energy (LCOE) to assess the cost-competitiveness of the RED optimal designs. The LCOE is the average revenue per unit of electricity generated needed to recover building and operating costs for a generation plant over a specific period and duty cycle, reflecting the overall competitiveness of different generation technologies.

2.4.1. Net and thermodynamic energy efficiency

The exergy or Gibbs free energy of mixing is the theoretical maximum energy that is available for useful work from a system reaching equilibrium. The difference in the Gibbs free energy between the final mixture and the initial high and low-salinity solutions yields the change in free energy of mixing of the inlet $\Delta G_{mix,in}$ and outlet $\Delta G_{mix,out}$ (8) streams of the RED process unit, *i.e.* streams (fso, rsu) and (rmu, dmi) [53,54].

$$\Delta G_{mix,i} = 2\ R\ T \sum_{sol\in\{HC,LC\}} Q_{i,sol}\ C_{i,sol}\ ln\frac{C_{i,sol}}{C_{M,i}} \tag{8}$$

$$\forall\ i \in in \cup out = (fso, rsu) \cup (rmu, dmi)$$

$$C_{M,i} = \frac{\sum_{sol\in\{HC,LC\}} Q_{i,sol}\ C_{i,sol}}{\sum_{sol\in\{HC,LC\}} Q_{i,sol}} \tag{9}$$

$$\forall\ i \in in \cup out = (fso, rsu) \cup (rmu, dmi)$$

where R is the gas constant (8.314 J/mol/K), T is the absolute temperature (K), 2 denotes the number of ions each NaCl molecule dissociates into, Q is the volumetric flowrate (m^3/s) and C the concentration (mol/m^3) of the initial high and low-salinity solutions entering and leaving the RED process. Equation (9) yields the concentration of the mixed solution in thermodynamic equilibrium (C_M in mol/m^3) of the RED process inflow and outflow streams.

The net energy efficiency, η_{net}, measures the input fraction of free energy that RED converts into electricity (10). The exergy change between RED process inlet and outlet streams is the exergy recovered for conversion, *i.e.*, the retrieved exergy for useful work ($\Delta G_{mix,retrieved}$), that is used to compute the thermodynamic efficiency, η_{th}, of the RED process, equation (11).

$$\eta_{net} = \frac{TNP}{\Delta G_{mix,in}} \tag{10}$$

$$\eta_{th} = \frac{TNP}{\Delta G_{mix,in} - \Delta G_{mix,out}} = \frac{TNP}{\Delta G_{mix,retrieved}} \tag{11}$$

2.4.2. Levelized Cost of Energy (LCOE)

The LCOE (€/kWh) estimates the average cost per unit of energy generated during the lifetime of a power plant that would break even the RED project costs. The LCOE gives a first-order assessment of the RED project viability. Assuming the energy provided annually is constant during the lifetime of the project, the LCOE reduces to (12).

$$LCOE = \frac{CRF{\cdot}CAPEX + OPEX}{TNP\ 8760\ LF} - cp{\cdot}ef \tag{12}$$

2.5. Specifications for the RED optimal design deployed in a desalination plant

Fig. 2 illustrates RED process integration with desalination and wastewater treatment plants and Table 2 reports the site-specific conditions of the case study. The large-scale RED system recovers energy from the concentrate effluent of Maspalomas II SWRO desalination plant in Gran Canaria (Canary Islands, Spain) [55–58]. Maspalomas II plant produces 26,184 m^3/day of desalted water with a SEC of 3.77 kWh/m^3. Nearby wastewater treatment plants (*e.g.*, el Tablero, las Burras) supply the low-salinity feedwater [58,59]. We assume the same LC and HC feed volume available for SGE conversion.

The case study explores how (i) electricity and carbon prices, (ii) membrane price, (iii) desalination plant capacity, and (iv) membrane resistance, may affect the cost-competitiveness, power density, and energy efficiency of the NPV-optimal RED design. Additionally, we assess the benefits of the GDP optimization model over trial-and-error approaches by comparing the traditional series-parallel layout to the optimal design that incorporates reuse and recycling of RED stacks outlet streams. All the assessments refer to a commercial RED unit (Table 3) in 2022, unless otherwise stated.

To assess the influence of electricity price and carbon pricing over time, we gather Spanish average electricity price [44] and EU ETS

Table 1
Financial parameters for the RED plant [48].

Parameter	Value
Plant lifetime, LT (years)	30
Membranes' lifetime, LT_m (years)	10
Load Factor, LF	90 %
Discount rate, DR	5 %
Spanish emission factor, ef (kg CO_2-eq/kWh)	0.374

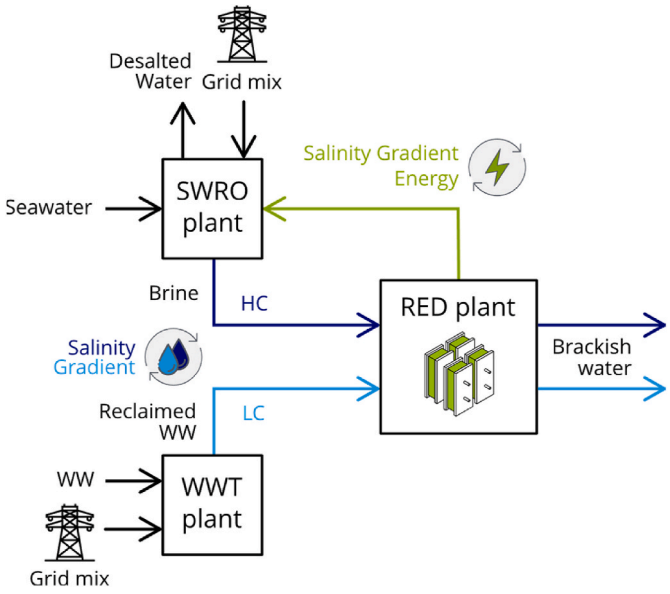

Fig. 2. RED-based energy recovery from the salinity gradient between seawater reverse osmosis (SWRO) desalination concentrate effluent (HC) and reclaimed wastewater (WW) effluents from WW treatment plants (LC).

Table 2
High-salinity (HC) and low-salinity (LC) feedwater properties.

Feedwater	HC	LC
Source	Maspalomas II SWRO plant	El Tablero and las Burras WW treatment plants
Flow rate (m^3/h)	733	733
NaCl concentration (M)	1.67	0.02

Temperature 20 °C.

Table 3
Parameters of the commercial RED stack (Fumatech GmbH®, Germany) [40].

Parameter	Value
Number of cell pairs	1000
Channel size	1.824 m × 1.532 m[a]
Spacers	
Thickness (μm)	270[b]
Porosity	82.5 %
Membranes properties: fumasep® CEM (FKS-50)/AEM (FAS-50)	
Areal resistance (Ω·cm^2)	1.8/0.6[c] (−20 %)[d]
Permselectivity (−)	0.93
Thickness dry (μm)	50
Active area (m^2)	0.7[a]

[a] Four times the size of fumatech® ED-1750 pilot-scale module.
[b] Equal to inter-membrane distance, *i.e.*, HC or the LC channels height.
[c] Measured in 0.5 M NaCl at 25 °C.
[d] Reduction assuming future advances in membranes design.

average emission allowances price [46] for the period 2017–2022. We regress EU-27 data from 2007 onwards [44] to estimate 2030 electricity prices; the carbon price in 2030 is a central estimate benchmark from OECD [60]. We assess the sensitivity to membrane costs by setting values between the current price of membranes (*i.e.*, average CEM and AEM cost from Fumatech®, 87.5 €/m^2) and the lowest price reported in the literature (~10 €/m^2) [61]. We reduce the flowrate of both HC and LC feedwaters to estimate the minimum SWRO desalination plant capacity that would allow the NPV-optimal RED process earn profits. We assume 20 % drop in membranes resistance to reflect future advancements in membranes design.

To evaluate the benefits of the GDP optimization model in RED process design over heuristic approaches, we compare two hydraulic arrangements each with the same number of candidate RED units (*i.e.*, $N_r = 35$):

(i) Fixed series-parallel layout, from our previous assessment [41], where the RED system treats desalination concentrate into several identical parallel arrays of units in series, so neither recycling nor alternative reuse of the outlet streams is allowed. The objective is to maximize the total net power of the parallel branch, as it was set in our previous study [41].
(ii) GDP layout, leaving the connection between the superstructure units free as a discrete decision. In this case, the objective is to maximize the NPV.

In the Series layout, we estimate the working conditions that maximize the net power of a stand-alone RED stack to fix the flowrate of the inlet streams to each parallel branch. We assume that the high and low salinity feedwaters are evenly split among the parallel branches, each with the same optimal configuration, so the net power output and costs of the RED system scale accordingly.

3. Results and discussion

For all the scenarios and the given parameters, each solution provides the NPV-optimal topology and decision variables that balance electricity production and capital and operating outlays increase. Discrete decisions include the working RED units and the active water streams. Continuous decisions are the flowrate and concentration of the inlet streams and the electric current of each active RED stack.

It is worth noting that simplifications and assumptions of the RED stack model [40] result in an overestimation of the net power output and, as such, an underestimation of the LCOE and an overestimation of the NPV. Besides, detailed and long-term electricity price data is essential in accurately evaluating the financial viability of renewable energy investments. Yet, there are significant hurdles to overcome that the electricity price regression to 2030 in this work does not fully address: balancing long-term time frames with fine time resolutions; forecasting electricity and carbon prices in future energy and market scenarios or unfamiliar pricing structures; and uncertainty in the price drivers [62].

3.1. Electricity and carbon price assessment

As expected, the upward trend of electricity and emissions allowances prices over time (Fig. 3, semi-log graph) favors RED process techno-economic performance (Fig. 4), which in turn relieves the grid mix supply of Maspalomas II desalination plant (RED-based electricity could meet about ~7–8% of the SEC). The optimal process designs feature power densities between 1.8 W/m^2 and 2.1 W/m^2 (markers labels, Fig. 4) and thermodynamic efficiencies ranging from 39 % to 42 % (markers color, Fig. 4).

Russia's invasion of Ukraine in early 2022 brought severe disruptions in the EU energy market. The unprecedent surge in European fossil gas prices is echoed in the unparallel electricity price spike in 2022 (Fig. 3), soaring prices that incentivizes the promotion of emerging renewable technologies such as RED. Besides, the cap-and-trade EU ETS limits the volume of allowances in the market over time (Fig. 3) to comply with emissions reduction targets, the scarcity of emission allowances (among other factors) increases their price used in financing RED (Fig. 5).

For the assessed period (Fig. 5), electricity sales are the main source of revenue, with lower yet growing revenue shares from auctioning allowances in the EU ETS (*e.g.*, from 1 % of all revenues in 2017 to ~11 % in 2022 and ~17 % in 2030). As a result, RED benefits grow by about 52 % in five years, a 25 % increase in NPV (Fig. 4). Despite the slight decline

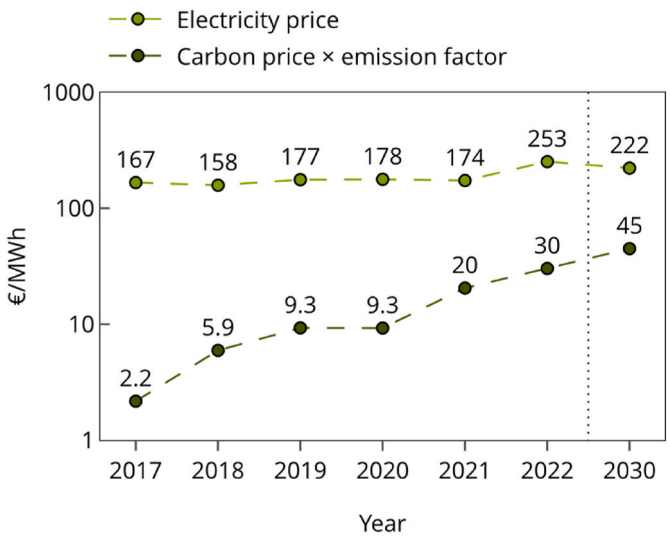

Fig. 3. Revenues per MWh from electricity and emission allowances over the period 2017–2022 with projections to 2030.

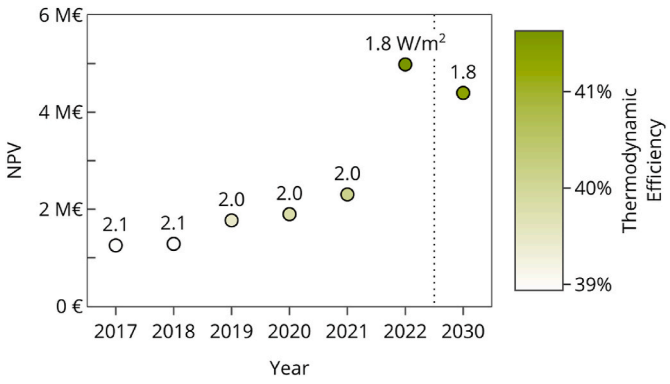

Fig. 4. Net present value, net power density (markers text), and thermodynamic energy efficiency (markers color) of the NPV-optimal RED process design over the past five years from 2022 and forecast to 2030.

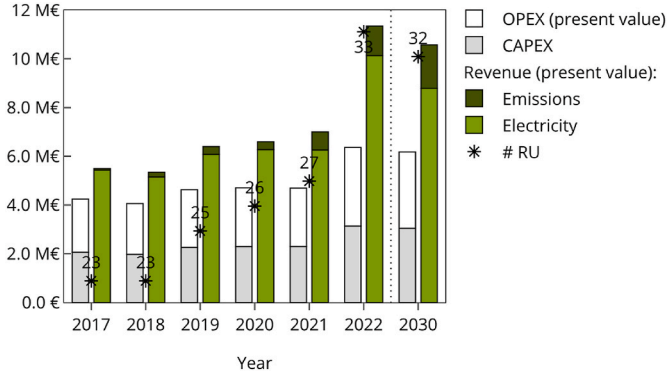

Fig. 5. NPV-optimal RED process over the period 2017–2022 with projections to 2030: cost and revenues breakdown in present value and number of active RED units, # RU.

of electricity price in 2030, the RED process may raise 724,155 euros each year during their lifetime yielding a NPV of about 4.4 million euros (Fig. 4).

When electricity is priced high, the revenue gained outstrips the increase in costs from a larger number of RED units (Fig. 5). The optimal solution therefore activates more RED units to raise the nominal generation capacity of the RED system (10 units in five years delivering 23 % more TNP), but at a cost. Each unit added to the RED system reduces the overall net power density from 2.1 W/m^2 in 2017 to 1.8 W/m^2 in 2022 (markers label, Fig. 4). On the flip side, the RED system retrieves more exergy for conversion (15 % more exergy than in 2017) from which a greater share (39 % in 2017 and 42 % in 2022) is converted into net electricity, enhancing the overall energy efficiency and net power output of the RED system (markers color, Fig. 4).

The overall net power density loss is related to the lower inlet flowrate of the RED units. This is because the same HC and LC feed volumes (kept constant throughout the years) are sourced to a larger number of RED units. Such lower inlet flowrate causes the RED units to depart from the net-power optimal working conditions, thereby reducing its power rate.

These findings indicate that in a context of high electricity prices and strong green financial support, RED technology does not require to reach the ambitious ~2.0 W/m^2 to be competitive as previous studies suggested. This is a reassuring result for RED transition from lab-scale to commercialization.

3.2. Membrane price assessment

The membrane price that breaks even the NPV-optimal RED design falls somewhere between 23 €/m^2 and 24 €/m^2 (Fig. 6), just under twice to six times the price of previous estimates of similar feeds concentrations (see Table 3).

Membranes priced above 23 €/m^2 yield larger economic losses when more than one RED unit is active, that is, the capital and operational expenses overshadow incomes from electricity sales and green financing incentives to a greater extent with an increasing number of working RED units (Fig. 7, semi-log graph); therefore, the optimal RED process design keeps one RED unit active under near-optimal working conditions (*i.e.*, maximum net generation), which results in a higher power density of 2.4 W/m^2 but reduced net (21 %) and thermodynamic (36 %) efficiencies (Fig. 8). As a result, the net power output and the derived electricity and emissions revenues from a single RED unit remain unchanged, whereas the investment and operational costs (*i.e.*, membranes' replacement cost) increase linearly with membrane price (Fig. 7). The balance between the constant revenues and higher total costs of a single but costlier RED stack is reflected in the linear decline of NPV with membrane price (Fig. 6).

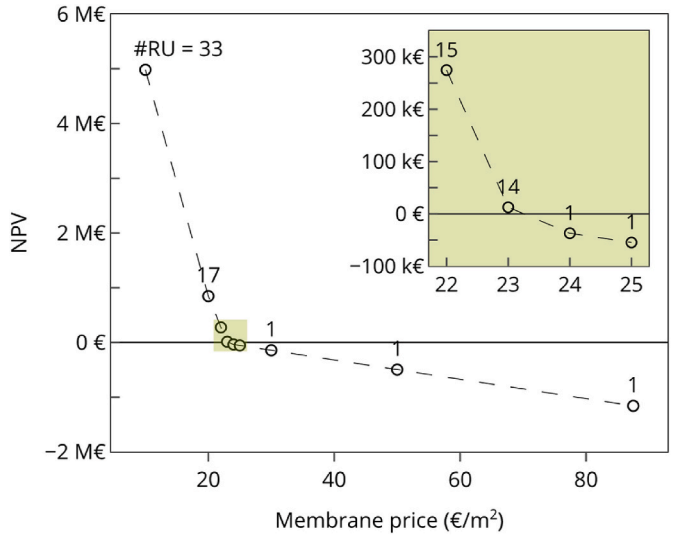

Fig. 6. Membrane price influence on the NPV-optimal RED process design: net present value and number of active RED units. The inset magnifies the NPV in the membrane price range within the boxed part of the graph.

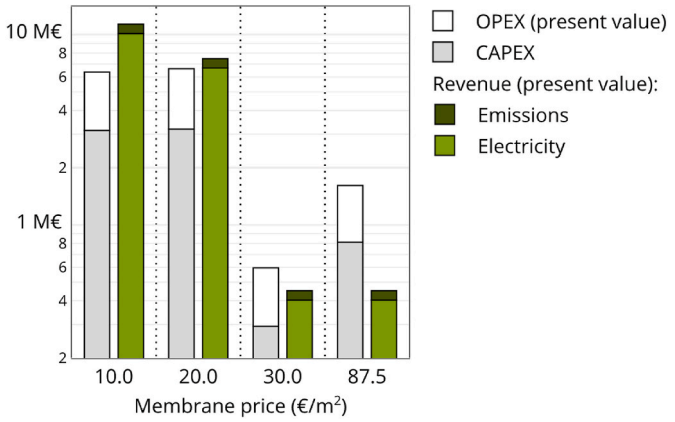

Fig. 7. Membrane price influence on the NPV-optimal RED process design: cost and revenues breakdown in present values.

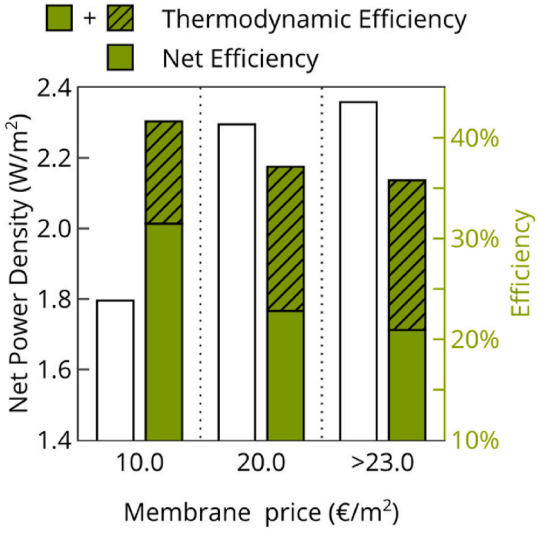

Fig. 8. Membrane price influence on the NPV-optimal RED process design: net power density, net and thermodynamic energy efficiencies.

The NPV trend shifts for membranes rated below 23 €/m^2, following a steep increase with lower membrane prices (Fig. 6). As membrane price falls the GDP model activates more RED units since the revenues earned outweigh the increase in capital and operating cost. The overall net power density decreases due to the larger number of RED units fed with the same feed flowrate, which recover a larger fraction of the input exergy for conversion increasing the net efficiency (Fig. 8). The thermodynamic efficiency also increases because the active RED units operate at lower inlet flowrates, reducing the overall pump power consumption.

With the reduction of membrane costs, designers can focus on achieving higher energy recovery rates from SG, leading to the development of more efficient and economically viable designs that increase the RED-based share of the SWRO desalination plant supply from 0.3 % from a single costlier RED unit to 8 % from 33 cheaper RED units. The scale-up of the RED process capacity to the MW order would likely make the project profitable in the short run if cheaper manufacturing membrane processes lower its cost to ~20 €/m^2.

3.3. SWRO desalination plant capacity assessment

The available feeds flowrate restricts the exergy input which in turn bounds the useful work of the RED process. The exergy input scales linearly with the desalination plant capacity (Fig. 9), and so does the TNP of the RED plant (Fig. 9 and markers size in Fig. 10). As such, to maximize the NPV with scarce feed volumes, the GDP optimization model deactivates RED units (keeping a single RED unit in the low-end capacity range of medium-sized SWRO desalination plants, *i.e.*, 500 m^3/day). By reducing the number of RED units, the NPV-optimal RED process attempts to emulate the overall working conditions with larger feed volumes. With larger HC and LC feed volumes (4400–17,600 m^3/day) the NPV-optimal solution retrieves ~76 % and converts ~31 % of the input exergy into electricity (TNP, Fig. 9). The net power density and thermodynamic efficiency (Fig. 10) remain roughly constant at ~1.8 W/m^2 and ~42 % up to a tenth of Maspalomas II capacity. owing to the lower number of RED units (3 units) operating with larger, net-power optimal flowrates that increase the net power density to 1.9 W/m^2 with a slight decline in thermodynamic efficiency (41 %).

Desalination plants rejecting ~334 m^3/day (*i.e.*, 500 m^3/day nominal capacity), would allow to install a single RED unit, that must run with a lower sub-optimal flowrate due to the scarce HC and LC feed flowrates, as such the net power density decreases to 1.4 W/m^2, while the energy efficiency increases to 44 % (Fig. 10). This is because the RED unit depletes to a greater extent the concentration gradient with lower hydrodynamic losses. Even so, the RED unit would source about 7.5 kW to the desalination plant with a profit of 53,595 euros.

Overall, the integration of on-site electricity generation based on RED technology in desalination plants of up to 500 m^3/day capacity can alleviate the reliance on water and energy-intensive grid mixes, contributing to more sustainable and self-sufficient water supply systems.

3.4. Membrane resistance assessment

The use of high-performance membranes would provide slightly more powerful—*i.e.*, 7.4 % more TNP with a 4.2 % increase in the overall net power density (Fig. 11)—and efficient designs—3.5 % more efficient in terms of thermodynamic efficiency (Fig. 11)–by simply adding a RED unit to the RED system (about 5.6 km^2 of total IEM area in a single stack). Such a small improvement would add up almost a million euros of benefits with virtually no impact on capital and operational costs, resulting in a 13 % NPV increase (Fig. 12). The LCOE would also improve, moving from 103 €/MWh to 97 €/MWh. These results emphasize that any improvement in membranes' performance has a positive impact on cost-competitiveness and widespread adoption of RED, a solid reason to thrust the development of cost-effective manufacturing processes and mass production of low-resistance membranes to reach prices of ~10 €/m^2.

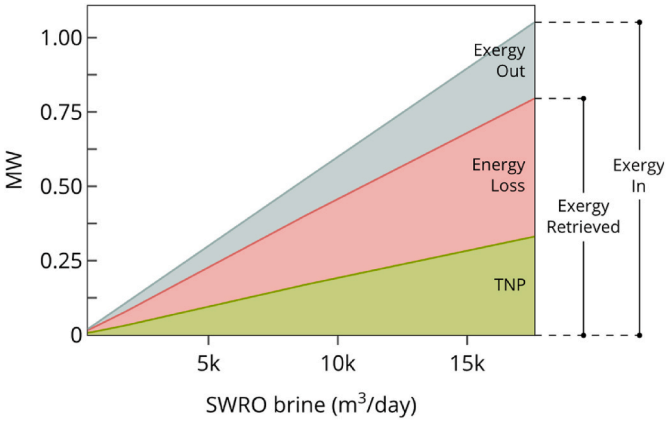

Fig. 9. SWRO desalination plant capacity influence on the NPV-optimal RED process design: energy balance.

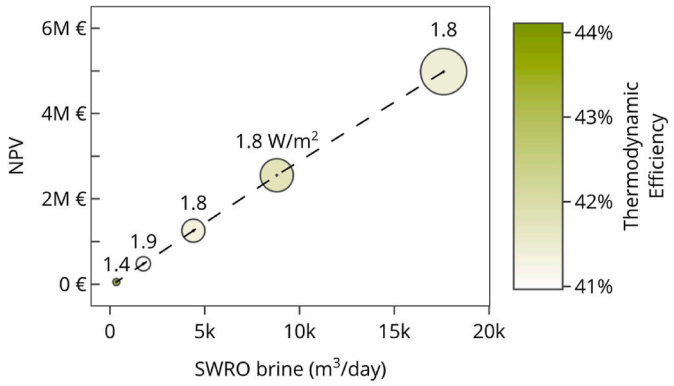

Fig. 10. SWRO desalination plant capacity influence on the NPV-optimal RED process design: net present value, net power density (markers text), total net power output (markers size), and net thermodynamic efficiency (markers color).

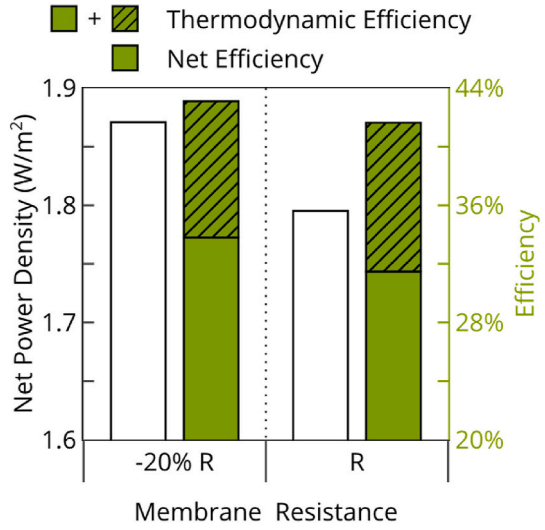

Fig. 11. Membrane resistance influence on the net power density, net and thermodynamic energy efficiencies of the NPV-optimal design.

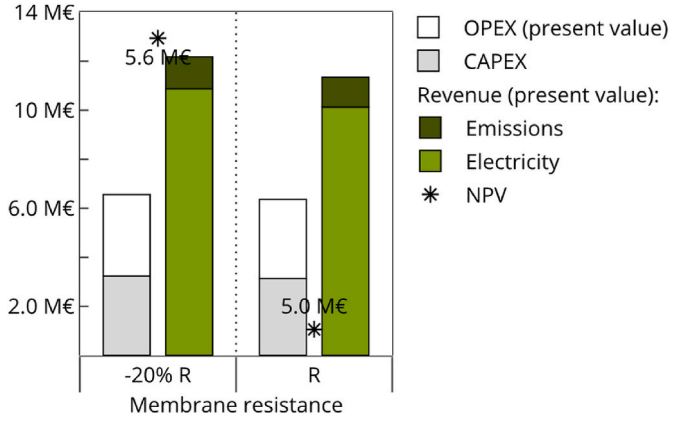

Fig. 12. Membrane resistance influence on the NPV-optimal design: cost and revenues breakdown in present values and net present value (markers).

3.5. Conventional series-parallel layout vs. NPV-optimal layout

The optimal GDP layout outperforms the series-parallel arrangement, as it renders economically viable RED process designs with almost equal energy and emissions savings from the grid (~7 % in the conventional layout and ~8 % in the cost-optimal layout).

The optimal series-parallel design of the RED process that peaks the total net power output with (i) a fixed hydraulic arrangement of the RED units, (ii) fixed concentration and flowrate of the HC and LC inlet water streams, and (iii) leaving the number of working RED units and its electric current as single decision variables, is far from being profitable (negative NPV of 2.9 million euros, Fig. 13). The GDP optimization model activates the largest feasible number of RED units in series, *i.e.*, 5 out of the 35 candidate RED units per parallel branch, to maximize the net power generation of the whole system. Even though the last RED units in the series increase the net power of the system, the RED unit's net power density well decreases from the first 1.9 W/m^2 to the last ~7 mW/m^2, which makes them prohibitively expensive.

While the net energy efficiency of the series layout (33 %, Fig. 14) aligns with the estimated value to make RED technology competitive with other renewables (*i.e.*, 40 %) [19], the total net power density (0.9 W/m^2, Fig. 14) falls well below the estimated value to make RED cost-competitive (2.0 W/m^2) [19]. The capital and operational expenses outweigh the benefits from electricity sales and green financing incentives which cover 78 % of the total costs, as seen in Fig. 13.

These results show that the optimal design from the technical perspective is not always the same from an economical viewpoint. The series configuration recovers a larger fraction of SGE at expense of lower power density that renders the RED process unprofitable.

Even though the conventional layout retrieves more energy for conversion (by increasing the extent of mixing through the series), the input exergy is lower than the optimal GDP layout (Fig. 15). This is because the total LC feed (assumed equal to Maspalomas II's desalination brine, ~733 m^3/h) restricts the number of parallel branches to 11. The optimal net-power inlet flowrate is about 0.6 times lower than the inlet LC flowrate. As such, around 42 % of the brine remains untapped reducing the input exergy of the RED system to 866 kW (Fig. 15).

As opposed to the series arrangement, the GDP layout, with its (i) larger volume of HC and LC feeds, and (ii) recycling and additional reuse alternatives, provides cost-optimal designs that can earn large profits (Fig. 13) while reconciling high efficiency and higher power densities (Fig. 14). The reduced extent of mixing and lower pump consumption of the GDP layout (Fig. 15) improves the thermodynamic energy efficiency which increases from 35 % in the series-parallel arrangement to 42 % in the GDP layout (Fig. 14) despite the larger fraction of exergy unused (Fig. 15), which yields a modest decrease in net efficiency (Fig. 14).

In the series-parallel arrangement, we enforce all RED units to work with higher flow velocities, those that peak the net power of the stand-

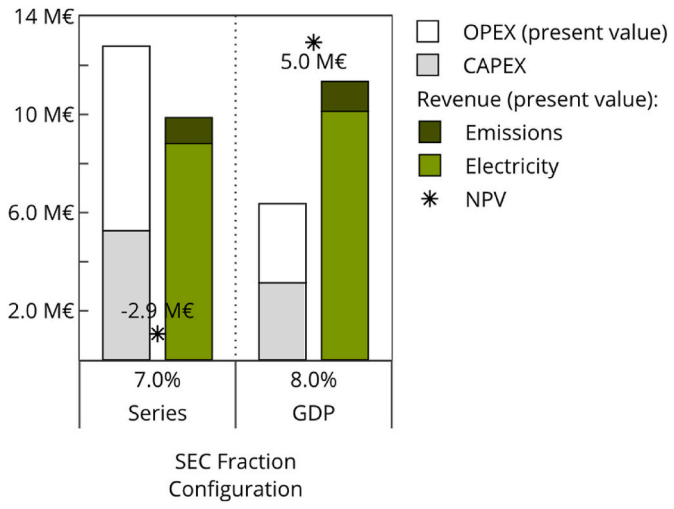

Fig. 13. Cost and revenues breakdown in present value and net present value of the series-parallel and NPV-optimal layouts.

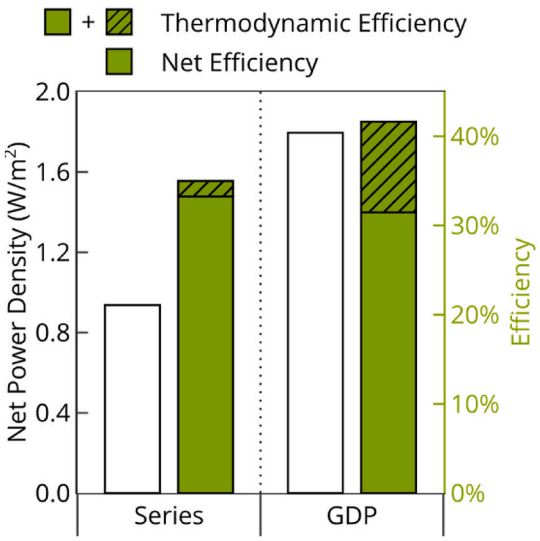

Fig. 14. Overall net power density, thermodynamic efficiency, and net energy efficiency of the series-parallel and NPV-optimal layouts.

alone RED unit (2.6 cm/s in the HC and 4.5 cm/s in the LC compartments). The effect of such high velocities is twofold: an overall pump power increase (eight times the GDP's), which in turn raises the investment and running costs (Fig. 13) and lowers the energy conversion efficiency (Loss in Fig. 15, and thermodynamic efficiency in Fig. 14).

These results underscore the value of mathematical programming and higher-level GDP modeling over heuristics for determining cost-optimal RED flowsheet designs.

3.6. Contextualizing RED economic competitiveness

Despite the discrepancy between the assumptions and scale of renewables projects (*i.e.*, utility-scale projects of at least 1 MW) in IRENA's LCOE estimates [63] and the NPV-optimal LCOE of RED, Fig. 16 provides some insights into RED competitiveness.

The assumed low membrane cost of 10 €/m^2 in all the assessed years would make the LCOE of the NPV-optimal RED design fall within the range of fossil fuel-fired power generation technologies (Fig. 16). In the face of soaring electricity prices and stiff emission reduction targets to be on track of 2030 Paris Agreement's goals, the NPV-optimal RED process would even be on par (*i.e.*, concentrated solar power, CSP) or in the range of other renewables.

If similar trends of steep cost reduction, technological advancements, and high penetration rates were to occur in RED technology, it is plausible that the LCOE for RED could reach levels comparable to established renewable technologies such as solar photovoltaic (PV) or onshore and offshore wind. This is in line with the steep cost reductions witnessed in solar PV, CSP, and offshore wind over the past decade (Fig. 16). Even though IRENA's analysis excludes the impact of government incentives or subsidies, carbon emission pricing or the benefits of renewables in reducing other externalities, these figures highlight the need to prove and advance RED to reach market readiness.

Table 4 compares reported cost estimates of RED and the LCOE of the NPV-optimal RED process designs for current and future membrane price scenarios in 2022. The lack of detailed economic evaluations and wide variability in LCOE (16–4956 €/MWh) across existing studies due to disparity in their underlying financial and process assumptions, makes any comparison inconclusive and open to discussion. As such, it serves to extract some general guidelines and trends.

The HC and LC feed concentration, volume, and temperature determine the input exergy and, thus, the nominal capacity and cost of the RED process. HC sources such as brines from coal mines, desalination, saltworks, salt lakes, or regenerated thermolytic salt solutions used in the so-called RED heat engines (1–5 M), offer higher SGE potential than less salty water bodies such as seawater (0.5–0.6 M). A purposely designed RED system could efficiently exploit these high-salinity sources, thus, reducing the LCOE.

Depending on the source, the feeds purity may also affect the performance and durability of RED if not properly pre-treated, which may increase capital and operational expenses. In this work, the objective function, *i.e.*, the NPV, excludes the pre-treatment cost, which is likely to result in an underestimation of the actual LCOE for RED systems that use sources with extensive pre-treatment requirements, *e.g.*, treated wastewater effluents, raw seawater, or river water.

None of the reported cost estimates in Table 4 consider the working conditions of each RED stack and their relative arrangement that may greatly improve both the performance and cost of the RED process as seen in the case study. Instead, most of them derived the cost of RED electricity or the LCOE for an estimated or projected RED unit power density or a targeted nominal capacity of the RED plant. Some also considered the impact of availability, concentration, and fouling potential of the HC and LC feeds, different RED stack sizes, and IEMs properties on RED system costs under fixed, suboptimal working conditions of the RED units. Such detailed assessments, however, miss cost-optimal design alternatives that optimization-based approaches can

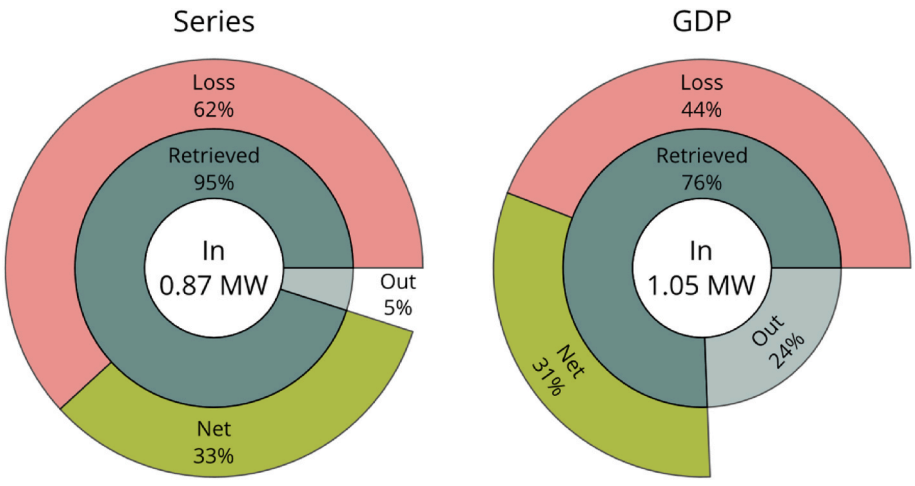

Fig. 15. Energy balance of the series-parallel and NPV-optimal layouts. In: Gibbs free energy entering the RED system. Out: Gibbs free energy leaving the RED system unused. Retrieved: Difference between input and output Gibbs free energies used for conversion in the RED system. Loss: Gibbs free energy lost in energy conversion. Net: total net power output of the RED system.

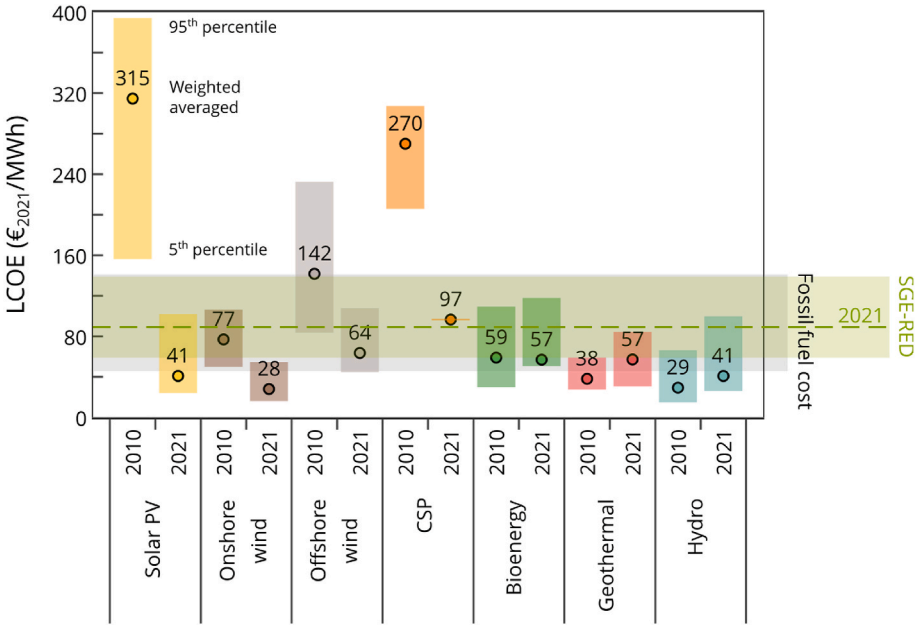

Fig. 16. Global LCOE from newly commissioned, utility-scale renewable power generation technologies, 2010–2020 [63]. NPV-optimal RED process LCOE range 2017–2022 and 2030 (green filled area) and 2021 LCOE (green dashed line). Grey filled area denotes price range of fossil fuel-fired technologies. All monetary values are in real, 2021 euros considering inflation and applying the exchange rate for each year. PV: photovoltaic; CSP: concentrating solar power.

Table 4
Cost estimates of RED reported in the literature and the present study. TP: Total power. PD: Power density. DR: Discount rate.

	High-salinity solution	Low-salinity solution	TP (MW)	PD (W/m^2)	Capacity Factor	Lifetime [years]		IEMs Price (€/m^2)[f]	DR	LCOE (€/MWh)[f]
						Plant	IEMs			
Turek (2007) [64]	0.6 M	9.6 mM	NR	0.46[a]	NR	NR	10	73 ($100/m^2)[c]	NR	4956 (6790)[e]
Turek (2008) [65]	1.9 M	9.6 mM	NR	1.04[a]	NR	NR	10	68 ($100/m^2)[d]	NR	2041 (3000)[e]
Post et al. (2010) [19]	0.5 M	5 mM	0.2	2[a]	91 %	20	7	2	6 %	79
								10		200
Daniilidis et al. (2014) [66]	0.5 M	17 mM	200	2.2[b]	84 %	25	7	4.3, 50	10	18, 71
				2.7[b]				4	%	16
Weiner et al. (2015) [67]	0.6 M	17 mM	NR	1.2[b]	NR	20	NR	676 ($750/m^2)[c]	6 %	5705 (6330)
Bevacqua et al. (2017)[g]	2.6 M NH_4HCO_3	75 mM NH_4HCO_3	0.1[a]	4.30	91 %	20	NR	50	6 %	683
[68]	2.4 M NH_4HCO_3	10 mM NH_4HCO_3		2.39						306
	2.5 M NH_4HCO_3	40 mM NH_4HCO_3		4.06						436
Micari et al. (2019)[g] [69]	5 M	10 mM	1[b]	3.2	90 %	30	10	30	5 %	400
Papapetrou et al. (2019)[g]	3.8 M	10 mM	0.1	0.66[b]	90 %	30	10	30	5 %	1360
[70]	5 M	10 mM	1	4.67[b]						210
Giacalone et al. (2019)	1.2 M	17 mM	2[b]	1[a]	90 %	30	10	15	5 %	500
[48]	5 M	<103 mM	4[b]	2[a]				4, 15		110, 250
			0.01–1[b]	1.5–2[a]				15		270–330
			0.04–3[b]	6.5[a]				4		30–50
Ranade et al. (2022) [71]	5 M	0.5 M	0.015	1.19[b]	82 %	20	10	5, 50	5 %	250, 1500
			0.031	2.44[b]						120,750
This work[h]	1.67 M	20 mM	0.327	1.8[b]	90 %	30	10	10	5 %	98
			0.013	2.3[b]				87.5		998

[a] Gross power.
[b] Net power.
[c] Total investment cost.
[d] Including endplates and electrodes.
[e] Cost of electricity.
[f] Values between brackets in US $ converted to € with the corresponding year average exchange ratio from the International Monetary Fund.
[g] RED heat engine.
[h] Circa 2022.

effectively handle and identify.

The case study and the reviewed studies reveal that realizing high-performing (*i.e.*, low-resistant, high-permselective), affordable membranes is a crucial lever for RED techno-economic progress toward market competitiveness. As shown in the case study, membrane cost weighs heavily on the objective function. Even though all scenarios have equal feedstreams conditions and candidate RED units, the high price of commercial membranes makes the NPV-optimal design uneconomic. Only if IEMs were one-order-of-magnitude cheaper, such that revenues offset the outlays increase, the NPV-optimal design would retain more RED units tuning their working conditions such that they reach the net power density that maximizes the NPV. The cumulative experience in

operating and developing RED technology will likely decrease its LCOE to the estimated 66–126 €/MWh.

4. Conclusions

RED technology has great potential in solving the water-energy challenge but needs to prove that it can generate electricity reliably to gain the trust of investors and manufacturers to unlock economies-of-scale cost reduction. This work applies an optimization model to devise techno-economic viable RED process designs that support the leap from lab to market. The Generalized Disjunctive Programming (GDP) model allowed us to define the hydraulic topology and working conditions of a set of RED units to maximize the net present value of the RED process deployed in a medium-capacity seawater reverse osmosis plant.

We have estimated the energy and emissions savings from the grid RED-based electricity may offer to desalination exploring relevant factors involved in the cost-optimal design of the RED process, providing valuable insights:

(a) The growing electricity and emission allowance prices over time strengthen RED market readiness in niche applications such as desalination and wastewater treatment sectors, reaching LCOE of 66–126 €/MWh on par or in the range of other renewable and conventional power technologies.
(b) A realistic near-term reduction in membrane cost (~20 €/m^2) would make RED profitable.
(c) The NPV-optimal RED process design may reap profits in medium-capacity SWRO desalination plants of up to 500 m^3/day.
(d) The use of low-resistance, low-cost membranes does improve the cost-competitiveness of the RED process; a 20 % drop in membranes resistance would increase profits by 13 %.
(e) Recycling and reusing alternatives brings on RED process designs that attain profits, reduce grid mix emissions, and accommodate higher power densities and energy efficiencies. Indeed, with a slightly lower RED-based take of the total desalination energy demand (~7 % and ~8 % in the series-parallel and NPV-optimal layouts), the series-parallel layout is as efficient as the GDP layout at the expense of a significant drop in power density which bears large economic losses.

These assessments show that mathematical programming is an efficient and systematic modeling and optimization tool to assist early-stage research, and to identify optimal design and operation guidelines for full-scale RED implementation. A natural progression of this work is to incorporate in decision-making uncertainty from electricity and emission allowances prices and membrane cost through stochastic optimization [72] and sustainability criteria through multi-objective optimization coupled with life cycle assessment principles [38].

CRediT authorship contribution statement

C. Tristán: Writing – original draft, Visualization, Validation, Software, Methodology, Investigation, Formal analysis, Data curation, Conceptualization. **M. Fallanza:** Writing – review & editing, Supervision, Conceptualization. **I. Ortiz:** Resources, Funding acquisition. **R. Ibáñez:** Writing – review & editing, Supervision, Resources, Project administration, Funding acquisition, Conceptualization. **I.E. Grossmann:** Writing – review & editing, Resources, Methodology, Conceptualization.

Declaration of competing interest

The authors declare that they have no known competing financial interests or personal relationships that could have appeared to influence the work reported in this paper.

Acknowledgments

This work was supported by the LIFE Programme of the European Union (LIFE19 ENV/ES/000143); the MCIN/AEI/10.13039/501100011033 and "European Union NextGenerationEU/PRTR" (PDC2021-120786-I00); and by the MCIN/AEI/10.13039/501100011033 and "ESF Investing in your future" (PRE2018-086454).

Appendix A. Supplementary data

Supplementary data to this article can be found online at https://doi.org/10.1016/j.energy.2024.134005.

Data availability

Data will be made available on request.

References

[1] Tufa RA, Pawlowski S, Veerman J, Bouzek K, Fontananova E, di Profio G, et al. Progress and prospects in reverse electrodialysis for salinity gradient energy conversion and storage. Appl Energy 2018;225:290–331. https://doi.org/10.1016/J.APENERGY.2018.04.111.
[2] Logan BE, Elimelech M. Membrane-based processes for sustainable power generation using water. Nature 2012;488:313–9. https://doi.org/10.1038/nature11477.
[3] Van Vliet MTH, Wiberg D, Leduc S, Riahi K. Power-generation system vulnerability and adaptation to changes in climate and water resources. Nat Clim Chang 2016;6:375–80. https://doi.org/10.1038/nclimate2903.
[4] Adamovic M, Bisselink B, De Felice M, De Roo A, Dorati C, Ganora D, et al. Water – energy nexus in europe. Luxembourg: Publications Office of the European Union; 2019. https://doi.org/10.2760/968197.
[5] Rani A, Snyder SW, Kim H, Lei Z, Pan SY. Pathways to a net-zero-carbon water sector through energy-extracting wastewater technologies. Npj Clean Water 2022 51 2022;(5):1–17. https://doi.org/10.1038/s41545-022-00197-8.
[6] IEA. WEO-2016 Special Report. Water-Energy Nexus 2016. https://doi.org/10.1021/es2016632. Paris.
[7] van Vliet MTH, Jones ER, Flörke M, Franssen WHP, Hanasaki N, Wada Y, et al. Global water scarcity including surface water quality and expansions of clean water technologies. Environ Res Lett 2021;16:024020. https://doi.org/10.1088/1748-9326/ABBFC3.
[8] Schunke AJ, Hernandez Herrera GA, Padhye L, Berry T-AA. Energy recovery in SWRO desalination: current status and new possibilities. Front Sustain Cities 2020;2:9. https://doi.org/10.3389/FRSC.2020.00009.
[9] Cornejo PK, Santana MVE, Hokanson DR, Mihelcic JR, Zhang Q. Carbon footprint of water reuse and desalination: a review of greenhouse gas emissions and estimation tools. J Water Reuse Desalin 2014;4:238–52. https://doi.org/10.2166/WRD.2014.058.
[10] Jones E, Qadir M, van Vliet MTH, Smakhtin V, Kang S. The state of desalination and brine production: a global outlook. Sci Total Environ 2019;657:1343–56. https://doi.org/10.1016/J.SCITOTENV.2018.12.076.
[11] Voutchkov N. Energy use for membrane seawater desalination – current status and trends. Desalination 2018;431:2–14. https://doi.org/10.1016/j.desal.2017.10.033.
[12] Pistocchi A, Bleninger T, Breyer C, Caldera U, Dorati C, Ganora D, et al. Can seawater desalination be a win-win fix to our water cycle? Water Res 2020;182:115906. https://doi.org/10.1016/J.WATRES.2020.115906.
[13] Elimelech M, Phillip WA. The future of seawater desalination: energy, technology, and the environment. Science (80-) 2011;333:712–7. https://doi.org/10.1126/science.1200488.
[14] Bundschuh J, Kaczmarczyk M, Ghaffour N, Tomaszewska B. State-of-the-art of renewable energy sources used in water desalination: present and future prospects. Desalination 2021;508:115035. https://doi.org/10.1016/J.DESAL.2021.115035.
[15] Nam J-Y, Hwang K-S, Kim H-C, Jeong H, Kim H, Jwa E, et al. Assessing the behavior of the feed-water constituents of a pilot-scale 1000-cell-pair reverse electrodialysis with seawater and municipal wastewater effluent. Water Res 2019;148:261–71. https://doi.org/10.1016/J.WATRES.2018.10.054.
[16] Yasukawa M, Mehdizadeh S, Sakurada T, Abo T, Kuno M, Higa M. Power generation performance of a bench-scale reverse electrodialysis stack using wastewater discharged from sewage treatment and seawater reverse osmosis. Desalination 2020;491:114449. https://doi.org/10.1016/j.desal.2020.114449.
[17] Mehdizadeh S, Kakihana Y, Abo T, Yuan Q, Higa M. Power generation performance of a pilot-scale reverse electrodialysis using monovalent selective ion-exchange membranes. Membranes 2021;11:27. https://doi.org/10.3390/MEMBRANES11010027.
[18] Tedesco M, Hamelers HVM, Biesheuvel PM. Nernst-Planck transport theory for (reverse) electrodialysis: II. Effect of water transport through ion-exchange membranes. J Memb Sci n.d.;531:172–182. https://doi.org/10.1016/j.memsci.2017.02.031.

[19] Post JW, Goeting CH, Valk J, Goinga S, Veerman J, Hamelers HVM, et al. Towards implementation of reverse electrodialysis for power generation from salinity gradients. Desalin Water Treat 2010;16:182–93. https://doi.org/10.5004/dwt.2010.1093.
[20] IEA-OES. Annual report: an overview of ocean energy activities in 2022. 2023.
[21] Pattle RE. Production of electric power by mixing fresh and salt water in the hydroelectric pile. Nature 1954;174:660. https://doi.org/10.1038/174660a0. 660.
[22] Tedesco M, Cipollina A, Tamburini A, Micale G. Towards 1 kW power production in a reverse electrodialysis pilot plant with saline waters and concentrated brines. J Memb Sci 2017;522:226–36. https://doi.org/10.1016/j.memsci.2016.09.015.
[23] Chae S, Kim H, Gi Hong J, Jang J, Higa M, Pishnamazi M, et al. Clean power generation from salinity gradient using reverse electrodialysis technologies: recent advances, bottlenecks, and future direction. Chem Eng J 2023;452:139482. https://doi.org/10.1016/J.CEJ.2022.139482.
[24] Tian H, Wang Y, Pei Y, Crittenden JC. Unique applications and improvements of reverse electrodialysis: a review and outlook. Appl Energy 2020;262:114482. https://doi.org/10.1016/J.APENERGY.2019.114482.
[25] Li W, Krantz WB, Cornelissen ER, Post JW, Verliefde ARD, Tang CY. A novel hybrid process of reverse electrodialysis and reverse osmosis for low energy seawater desalination and brine management. Appl Energy 2013;104:592–602. https://doi.org/10.1016/j.apenergy.2012.11.064.
[26] Badruzzaman M, Voutchkov N, Weinrich L, Jacangelo JG. Selection of pretreatment technologies for seawater reverse osmosis plants: a review. Desalination 2019;449:78–91. https://doi.org/10.1016/j.desal.2018.10.006.
[27] Ciofalo M, La Cerva M, Di Liberto M, Gurreri L, Cipollina A, Micale G. Optimization of net power density in Reverse Electrodialysis. Energy 2019;181:576–88. https://doi.org/10.1016/J.ENERGY.2019.05.183.
[28] Long R, Li B, Liu Z, Liu W. Performance analysis of reverse electrodialysis stacks: channel geometry and flow rate optimization. Energy 2018;158:427–36. https://doi.org/10.1016/J.ENERGY.2018.06.067.
[29] Altıok E, Kaya TZ, Othman NH, Kınalı O, Kitada S, Güler E, et al. Investigations on the effects of operational parameters in reverse electrodialysis system for salinity gradient power generation using central composite design (CCD). Desalination 2022;525:115508. https://doi.org/10.1016/J.DESAL.2021.115508.
[30] Long R, Li B, Liu Z, Liu W. Reverse electrodialysis: modelling and performance analysis based on multi-objective optimization. Energy 2018;151:1–10. https://doi.org/10.1016/j.energy.2018.03.003.
[31] Veerman J, Saakes M, Metz SJ, Harmsen GJ. Electrical power from Sea and river water by reverse electrodialysis: a first step from the laboratory to a real power plant. Environ Sci Technol 2010;44:9207–12. https://doi.org/10.1021/es1009345.
[32] Hu J, Xu S, Wu X, Wu D, Jin D, Wang P, et al. Multi-stage reverse electrodialysis: strategies to harvest salinity gradient energy. Energy Convers Manag 2019;183:803–15. https://doi.org/10.1016/J.ENCONMAN.2018.11.032.
[33] Gao H, Li J, Fu R, Wang L, Wang H, Pan T, et al. The effect of flow modes on the capture of the energy between concentrated brine and seawater by reverse electrodialysis. Energy Convers Manag 2023;292:117357. https://doi.org/10.1016/J.ENCONMAN.2023.117357.
[34] Tedesco M, Mazzola P, Tamburini A, Micale G, Bogle IDL, Papapetrou M, et al. Analysis and simulation of scale-up potentials in reverse electrodialysis. Desalin Water Treat 2015;55:3391–403. https://doi.org/10.1080/19443994.2014.947781.
[35] Veerman J. Reverse electrodialysis: Co-and counterflow optimization of multistage configurations for maximum energy efficiency. Membranes 2020;10:1–13. https://doi.org/10.3390/membranes10090206.
[36] Simões C, Pintossi D, Saakes M, Brilman W. Optimizing multistage reverse electrodialysis for enhanced energy recovery from river water and seawater: experimental and modeling investigation. Adv Appl Energy 2021;2:100023. https://doi.org/10.1016/J.ADAPEN.2021.100023.
[37] Grossmann IE, Caballero JA, Yeomans H. Mathematical programming approaches to the synthesis of chemical process systems. Korean J Chem Eng 1999 164 1999;16:407–26. https://doi.org/10.1007/BF02698263.
[38] Guillén-Gosálbez G, You F, Galán-Martín Á, Pozo C, Grossmann IE. Process systems engineering thinking and tools applied to sustainability problems: current landscape and future opportunities. Curr Opin Chem Eng 2019;26:170–9. https://doi.org/10.1016/j.coche.2019.11.002.
[39] Grossmann IE, Trespalacios F. Systematic modeling of discrete-continuous optimization models through generalized disjunctive programming. AIChE J 2013;59:3276–95. https://doi.org/10.1002/aic.14088.
[40] Tristán C, Fallanza M, Ibáñez R, Ortiz I, Grossmann IE. A generalized disjunctive programming model for the optimal design of reverse electrodialysis process for salinity gradient-based power generation. Comput Chem Eng 2023;174:108196. https://doi.org/10.1016/j.compchemeng.2023.108196.
[41] Tristán C, Fallanza M, Ibáñez R, Ortiz I. Recovery of salinity gradient energy in desalination plants by reverse electrodialysis. Desalination 2020;496:114699. https://doi.org/10.1016/j.desal.2020.114699.
[42] Ortiz-Imedio R, Gomez-Coma L, Fallanza M, Ortiz A, Ibañez R, Ortiz I. Comparative performance of salinity gradient power-reverse electrodialysis under different operating conditions. Desalination 2019;457:8–21. https://doi.org/10.1016/J.DESAL.2019.01.005.
[43] Chen Q, Grossmann IE. Recent Developments and Challenges in Optimization-Based Process Synthesis 2017;8:249–83. https://doi.org/10.1146/ANNUREV-CHEMBIOENG-080615-033546. 101146/Annurev-Chembioeng-080615-033546.
[44] EUROSTAT. Electricity prices for non-household consumers - bi-annual data (from 2007 onwards) [NRG_PC_205] n.d. https://ec.europa.eu/eurostat/databrowser/bookmark/65f83096-1534-4ddc-a561-44764c07601c?lang=en (accessed April 3, 2023).
[45] Wernet G, Bauer C, Steubing B, Reinhard J, Moreno-Ruiz E, Weidema B. The ecoinvent database version 3 (part I): overview and methodology. Int J Life Cycle Assess 2016;21:1218–30. https://doi.org/10.1007/s11367-016-1087-8.
[46] ICAP. Allowance price explorer. https://icapcarbonaction.com/en/ets-prices. [Accessed 8 May 2023].
[47] Bartholomew TV, Siefert NS, Mauter MS. Cost optimization of osmotically assisted reverse osmosis. Environ Sci Technol 2018;52:11813–21. https://doi.org/10.1021/acs.est.8b02771.
[48] Giacalone F, Papapetrou M, Kosmadakis G, Tamburini A, Micale G, Cipollina A. Application of reverse electrodialysis to site-specific types of saline solutions: a techno-economic assessment. Energy 2019;181:532–47. https://doi.org/10.1016/j.energy.2019.05.161.
[49] Hart WE, Laird CD, Watson J-P, Woodruff DL, Hackebeil GA, Nicholson BL, et al. Pyomo — optimization modeling in Python. 67. second ed. Cham: Springer International Publishing; 2017. https://doi.org/10.1007/978-3-319-58821-6.
[50] Chen Q, Johnson ES, Bernal DE, Valentin R, Kale S, Bates J, et al. Pyomo.GDP: an ecosystem for logic based modeling and optimization development. Optim Eng 2022;23:607–42. https://doi.org/10.1007/s11081-021-09601-7.
[51] Lee S, Grossmann IE. A global optimization algorithm for nonconvex generalized disjunctive programming and applications to process systems. Comput Chem Eng 2001;25:1675–97. https://doi.org/10.1016/S0098-1354(01)00732-3.
[52] Chen Q, Johnson ES, Siirola JD, Grossmann IE. Pyomo.GDP: disjunctive models in Python. Comput. Aided Chem. Eng. 2018;44:889–94. https://doi.org/10.1016/B978-0-444-64241-7.50143-9. Elsevier B.V.
[53] Forgacs C. Recent developments in the utilization of salinity power. Desalination 1982;40:191–5. https://doi.org/10.1016/S0011-9164(00)88683-X.
[54] Veerman J, Saakes M, Metz SJ, Harmsen GJ. Reverse electrodialysis: a validated process model for design and optimization. Chem Eng J 2011;166:256–68. https://doi.org/10.1016/j.cej.2010.10.071.
[55] Meyer-Steele S, von Gottberg A, Talavera JL. New Sea water reverse osmosis plant for the caribbean "energy recovery, brine recovery & cost reduction.". 2001.
[56] Portillo E, de la Rosa MR, Louzara G, Quesada J, Ruiz JM, Mendoza H. Dispersion of desalination plant brine discharge under varied hydrodynamic conditions in the south of Gran Canaria. Desalin Water Treat 2014;52:164–77. https://doi.org/10.1080/19443994.2013.795349.
[57] Sadhwani Alonso JJ, Melián-Martel N. Environmental regulations—inland and coastal desalination case studies. In: Gude VG, editor. Sustain. Desalin. Handb. Plant sel. Des. Implement. Butterworth-Heinemann; 2018. p. 403–35. https://doi.org/10.1016/B978-0-12-809240-8.00010-1.
[58] Consejo Insular de Aguas de Gran Canaria. Plan hidrológico de Gran Canaria. Ciclo de Planificación 2021-2027. Demarcación hidrográfica ES120 GRAN CANARIA. 2023.
[59] Pérez Talavera J, Quesada Ruiz J. Identification of the mixing processes in brine discharges carried out in Barranco del Toro Beach, south of Gran Canaria (Canary Islands). Desalination 2001;139:277–86. https://doi.org/10.1016/S0011-9164(01)00320-4.
[60] OECD. Effective carbon rates 2021: pricing carbon emissions through taxes and emissions trading. Paris: OECD; 2021. https://doi.org/10.1787/0e8e24f5-en.
[61] Small Business Innovation Research (SBIR) and Small Business Technology Transfer (STTR) programs. Low-Cost Manufacturing of High-Performance Ion Exchange Membranes for Electrodialysis using Initiated Chem Vap Depos n.d. https://web.archive.org/web/20240528173426/https://www.sbir.gov/node/2282063 (accessed December 8, 2022).
[62] Gabrielli P, Wüthrich M, Blume S, Sansavini G. Data-driven modeling for long-term electricity price forecasting. Energy 2022;244:123107. https://doi.org/10.1016/J.ENERGY.2022.123107.
[63] IRENA. Renewable power generation costs in 2021. Abu dhabi. 2021.
[64] Turek M, Bandura B. Renewable energy by reverse electrodialysis. Desalination 2007;205:67–74. https://doi.org/10.1016/J.DESAL.2006.04.041.
[65] Turek M, Bandura B, Dydo P. Power production from coal-mine brine utilizing reversed electrodialysis. Desalination 2008;221:462–6. https://doi.org/10.1016/J.DESAL.2007.01.106.
[66] Daniilidis A, Herber R, Vermaas DA. Upscale potential and financial feasibility of a reverse electrodialysis power plant. Appl Energy 2014;119:257–65. https://doi.org/10.1016/j.apenergy.2013.12.066.
[67] Weiner AM, McGovern RK, Lienhard VJH. A new reverse electrodialysis design strategy which significantly reduces the levelized cost of electricity. J Memb Sci 2015;493:605–14. https://doi.org/10.1016/j.memsci.2015.05.058.
[68] Bevacqua M, Tamburini A, Papapetrou M, Cipollina A, Micale G, Piacentino A. Reverse electrodialysis with NH4HCO3-water systems for heat-to-power conversion. Energy 2017;137:1293–307. https://doi.org/10.1016/J.ENERGY.2017.07.012.
[69] Micari M, Cipollina A, Giacalone F, Kosmadakis G, Papapetrou M, Zaragoza G, et al. Towards the first proof of the concept of a reverse ElectroDialysis - membrane distillation heat engine. Desalination 2019;453:77–88. https://doi.org/10.1016/j.desal.2018.11.022.
[70] Papapetrou M, Kosmadakis G, Giacalone F, Ortega-Delgado B, Cipollina A, Tamburini A, et al. Evaluation of the economic and environmental performance of low-temperature heat to power conversion using a reverse electrodialysis – multi-

effect distillation system. Energies 2019;12:3206. https://doi.org/10.3390/en12173206.

[71] Ranade A, Singh K, Tamburini A, Micale G, Vermaas DA. Feasibility of producing electricity, hydrogen, and chlorine via reverse electrodialysis. Environ Sci Technol 2022;2022:16062–72. https://doi.org/10.1021/ACS.EST.2C03407/ASSET/IMAGES/LARGE/ES2C03407_0007.JPEG.

[72] Roald LA, Pozo D, Papavasiliou A, Molzahn DK, Kazempour J, Conejo A. Power systems optimization under uncertainty: a review of methods and applications. Electr Power Syst Res 2023;214:108725. https://doi.org/10.1016/J.EPSR.2022.108725.